Calphad 59 (2017) 189–198

Contents lists available at ScienceDirect

Calphad

journal homepage: www.elsevier.com/locate/calphad

Experimental investigation and thermodynamic calculation of the B-Fe-Mo ternary system

Xuemei Ou Yang[a,b], Fucheng Yin[a,b,*], Jingxian Hu[a,b], Manxiu Zhao[a,b], Ye Liu[a,b,c]

[a] School of Materials Science and Engineering, Xiangtan University, Xiangtan, Hunan 411105, PR China
[b] Key Laboratory of Materials Design and Preparation Technology of Hunan Province, Xiangtan University, Xiangtan, Hunan 411105, PR China
[c] State Key Laboratory of Powder Metallurgy, Central South University, Changsha, Hunan 430074, PR China

ARTICLE INFO

Keywords:
B-Fe-Mo system
Liquidus projection
Thermodynamic modeling
Phase diagram

ABSTRACT

The phase relationship of the B-Fe-Mo ternary system has been investigated combining experimental results with thermodynamic modeling. The liquidus projection of the ternary system in the Fe-rich region was constructed by identifying primary crystallization phases in the as-cast alloys and determining liquid temperatures obtained from the DSC analyses. Eight different primary solidification regions were observed, and they are BCC, FCC, Mo_2FeB_2, Fe_2B, FeB, σ, and R, respectively. And four invariant reactions were identified in the Fe-rich region. Thermodynamic optimization of the B-Fe-Mo ternary system was performed using CALPHAD approach based on the thermodynamic models of the three constitutional binary systems and the experimental results of the ternary system. A set of self-consistent thermodynamic parameters for the B-Fe-Mo system were obtained with reasonable agreement between the experimental and calculated results.

1. Introduction

The B-Fe-Mo system is an important subsystem in boron containing steels [1] and MoB steels [2,3], which are widely used in automobile industry as reinforced sheets used for doors, front bumpers and B-pillars. This system is also important for metallic glasses which display interesting properties such as good soft magnetic properties, high strength, good corrosion resistance, and so on [4–6]. Mo_2FeB_2 based cermets have attracted many attentions owing to their superior high-temperature properties and wide application prospect in the field of wear-resistance materials, such as injection machine parts, can making tools, and hot copper extruding dies [7,8]. B and Mo are the commonly used alloying elements that can improve the strength and corrosion resistance of many metallic (e.g., Al, Cu, Fe and Ni-based) materials. For example, Ouyang et al. [9] reported that adding 8 wt% Mo could increase the corrosion resistance of the Fe-3.5B alloy in the molten zinc by the improvement of borides stability and grain refining of eutectic borides.

Understanding the phase relations and thermodynamic properties of the alloy system is of particular interest in designing alloy compositions and processing methods. In the present work, experimental investigations using SEM, EPMA, DSC, and XRD were carried out on the solidified Fe-rich alloys to determine the species of primary phase, the temperatures of invariant reactions, and phase transformation processes during solidification. In addition, thermodynamic optimization of the ternary system was carried out using the CALPHAD method, based on the thermodynamic descriptions of the three constitutional binary systems and the experimental results of the ternary system.

2. Review of literature

2.1. B-Fe, B-Mo, and Fe-Mo binary systems

The equilibrium phases in the B-Fe binary system are liquid (L), BCC (α-Fe and δ-Fe), FCC (γ-Fe), rhombohedral B (βB), Fe_2B, and FeB, respectively. Four invariant reactions are proposed as: (I) L + BCC ⇔ FCC at 1667 K; (II) L ⇔ FCC + Fe_2B at 1447 K; (III) L + FeB ⇔ Fe_2B at 1662 K; (IV) L ⇔ FeB + (B) at 1662 K and (V) FCC ⇔ BCC + Fe_2B at 1185 K. In addition, Khan et al. [10] reported the formation of the metastable Fe_3B phase in the rapidly quenched samples, while Battezzati et al. [11] proposed that the metastable phase could change to a stable phase by the reaction, Fe_3B ⇔ Fe_2B + α-Fe. Thermodynamic description of the B-Fe system has been extensively reported [12–15]. More recently, Yoshitomi et al. [13] reassessed the B-Fe system by combining the first principles calculations and CALPHAD method. However, the predicted invariant reaction temperature of L ⇔ FeB + (βB) is about 43 K lower than the widely accepted value of 1773 K [14]. In the present work, the results obtained by Palumbo et al. [15], which are in well agreement

* Corresponding author at: School of Materials Science and Engineering, Xiangtan University, Xiangtan, Hunan 411105, PR China.
E-mail address: fuchengyin@xtu.edu.cn (F. Yin).

http://dx.doi.org/10.1016/j.calphad.2017.10.007
Received 20 August 2017; Received in revised form 26 September 2017; Accepted 17 October 2017

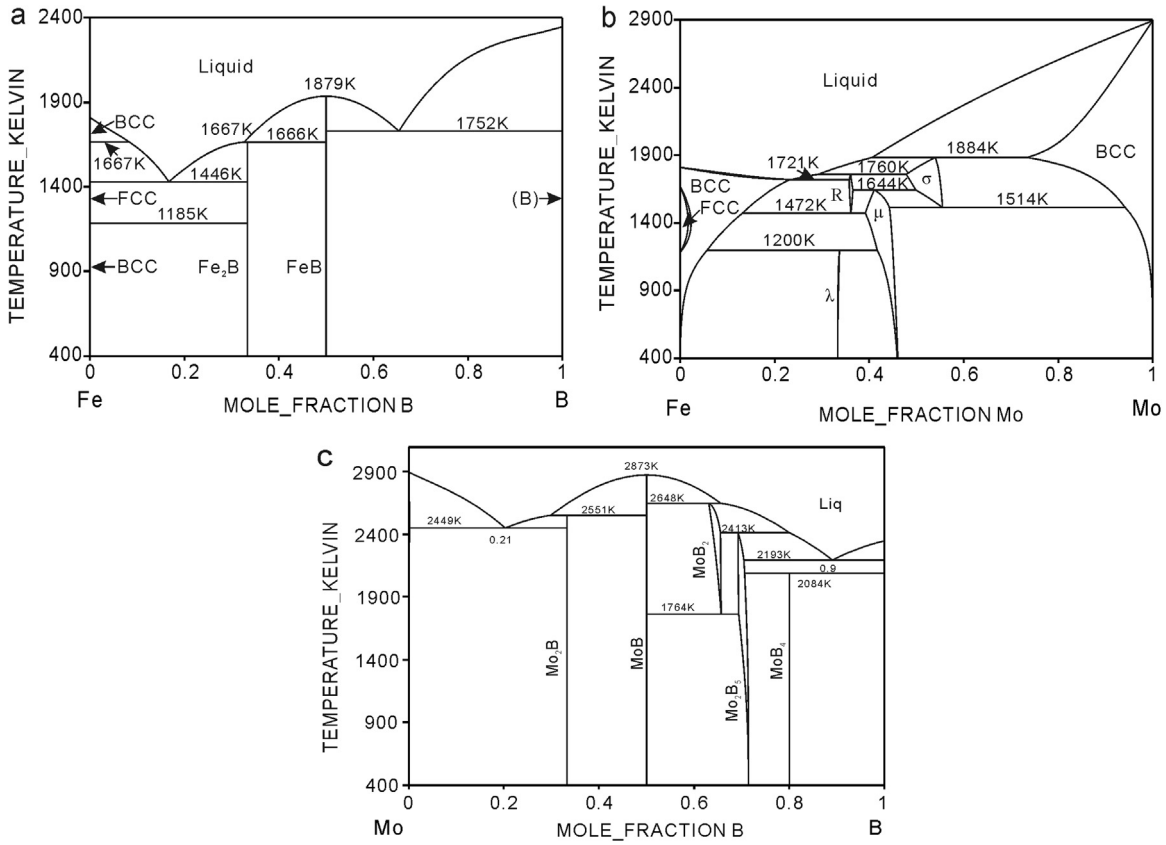

Fig. 1. Calculated phase diagrams of Fe-B system [15] (a), B-Mo system [20] (b), and Fe-Mo system [28] (c).

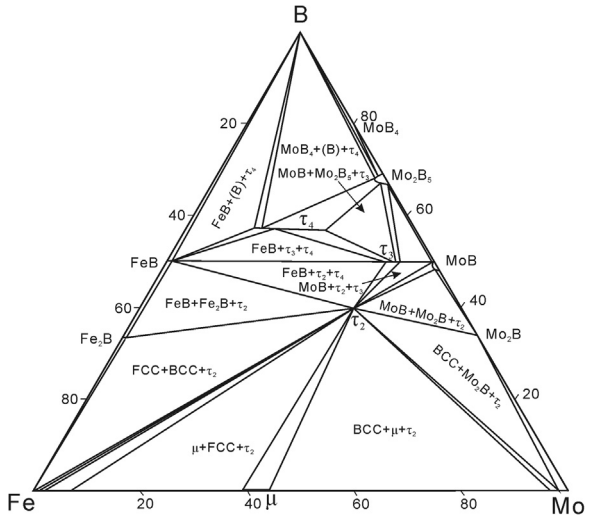

Fig. 2. Isothermal section at 1323 K amended by Korniyenko and Bondar [31].

with the experimental phase diagram, were adopted. The calculated B-Fe binary phase diagram is shown in Fig. 1a.

The phase equilibria of the Mo-B system were first reviewed by Brewer et al. [16] and later by Spear and Wang [17]. Spear and Liao [18] carried out a thermodynamic assessment for this system based on the results of Brewer et al. Then a reassessment was done by Morishita et al. [19], however, no thermodynamic parameters were reported. Recently, Yang et al. [20] reassessed this system during the calculation of the Mo-Si-B system. Five compounds, MoB_4, Mo_2B_5, MoB_2, MoB, and Mo_2B, were considered to be stable in this system. The calculated B-Mo phase diagram is show in Fig. 1b. Until now, αMoB and βMoB were treated as one phase during the Mo-B thermodynamic assessment for simplification. The invariant reactions, βMoB + Mo_2B ↔ αMoB at 2453 ± 50 K, and L + βMoB ↔ Mo_2B at 2553 ± 12 K were ignored.

Several authors have critically reviewed the experimental constitutional, crystallographic, and thermochemical data of the Fe-Mo system [21–24]. The thermodynamic assessment of the Fe-Mo system was carried out by some researches [25–28]. In the present work, the results obtained by Rajkumar et al. [28], considering the newly measured enthalpy increment data and the constitutional data, were directly used in the present work, and the calculated Fe-Mo phase diagram is shown in Fig. 1c. The results show that there are four intermediate phases in the system σ , μ , λ, and R, and three invariant reactions involving liquid: (I) L + σ ⇔ R at 1761 K; (II) L ⇔ α-Fe + R at 1722 K, (III) L + (Mo) ⇔ σ at 1884 K.

2.2. B-Fe-Mo ternary system

Only a few studies on the experimental determination of the B-Fe-Mo ternary system were reported. Isothermal sections at 1323 K were constructed by Haschke et al. [29] based on the results of X-ray diffraction and Leithe-Jasper et al. [30] using X-ray powder diffraction and electron microprobe analysis. Then it was amended by Korniyenko and Bondar [31] based on the experimental data of [30] and the accepted binary phase diagrams. The results are shown in Fig. 2. Gladyshevskii et al. [32] proposed the isothermal section at 1273 K, which is similar to the results of [31]. The main difference lies in the homogeneity ranges of ternary phases and the phase relationship at the Mo-rich corner.

Three linear ternary solid phases were found to be stable at 1323 K, τ_2-Mo_2FeB_2 with U_3Si_2-type structure, τ_3-$Mo_{1-x}Fe_xB$ with CrB-type structure, and τ_4-$Mo_{1+x}Fe_{2-x}B_4$ with Ta_3B_4-type structure, respectively. Haschke et al. [29] proposed the existence of τ_1-$Mo_2Fe_{13}B_5$ phase in a narrow temperature range, while a phase named $(Mo_{1-x}Fe_x)_3B$ with the same composition and structure as τ_1-$Mo_2Fe_{13}B_5$ and Fe_3B was

Table 1
Crystallographic data of the binary and ternary compounds.

Phase	Prototype	Space group	Lattice parameters(nm)			Temperature and Composition range
			a	b	c	
FeB	FeB	*Pnma*	0.5591	0.2958	0.4081	< 1876 K, dissolves ~ 1.8–2.5 at% Mo
Fe_2B	$CuAl_2$	*I4/mcm*	0.5110	0.5110	0.4240	< 1672 K, dissolves ~ 0.6–2.3 at% Mo
Fe_3B/τ_1	Ti_3P	$P4_2/n$	0.8631	0.8631	0.4311	Metastable phase
Mo_2B	$CuAl_2$	*I4/mcm*	0.5547	0.5547	0.4734	< 2553 K
αMoB	αMoB	$I4_1amd$	0.3110	0.3110	1.6950	< 2453 K, ~ 0.5 at% Fe dissolves
βMoB	CrB	*Cmcm*	0.3151	0.8470	0.3082	2073–2873 K
MoB_2	AlB_2	*P6/mmm*	0.3040	0.3040	0.3060	1790–2648 K
Mo_2B_5	Mo_2B_5	*R-3m*	0.3008	0.3008	2.0914	< 2413K, ~ 0.5–2.3 at% Fe dissolves
MoB_4	WB4	$P6_3/mmc$	0.5204	0.5204	0.6350	< 2080 K
μ-Mo_6Fe_7	W_6Fe_7	*R-3m*	0.4759	0.4759	2.5715	< 1672 K
R-Mo_2Fe_3	$Co_5Cr_2Mo_3$	*R-3*	1.9560	1.9560	1.9353	1473–1761 K
λ-Fe_2Mo	$MgZn_2$	$P6_3/mmc$	0.4755	0.4755	0.7767	< 1200 K
σ-FeMo	CrFe	$P4_2/mnm$	0.9188	0.9188	0.4812	1508–1884 K
τ_2-$FeMo_2B_2$	U_3Si_2	*P4/mbm*	0.5772	0.5772	0.3142	~ 20 at Fe and 40 at% B
τ_4-Fe_2MoB_4	Ta_3B_4	*Immm*	0.3152	0.8418	0.3066	~ 14–30 at% Fe with 57 at% B at 1323 K

found by Leithe-Jasper et al. [30]. Therefore, Fe_3B, $(Mo_{1-x}Fe_x)_3B$, and τ_1-$Mo_2Fe_{13}B_5$ were treated as one phase named as τ_1 in the following description, which is stable at 1353–1383 K in the present work. In addition, τ_3-$Mo_{1-x}Fe_xB$ has the same structure with βMoB, and was considered to be stabilized by dissolving Fe atoms to lower temperature. So τ_3-Mo1-xFexB was treated as the βMoB with a small Fe dissolution. The experimental data from Leithe-Jasper et al. [30] and Gladyshevskii et al. [32] were considered in the present work. The available information on the crystallographic data, temperatures and composition ranges of all compounds involved in the B-Fe-Mo system is summarized in Table 1.

Only limited data are available from the literatures on the thermal behavior of the ternary system. Ide and Ando [33] investigated the thermal behavior of three samples in the Fe-rich corner. In their work, liquid began to form above 1365 K by a eutectic-like reaction, then above 1415 K, a reaction including FCC and Mo_2FeB_2 occurred. Until now, the temperatures of the proposed invariant reactions were not measured.

It should be noted that no thermodynamic description on the ternary system is available. Isothermal sections of the B-Fe-Mo system for a boron content of up to 34 at% at temperatures of 1473 K and 1553 K were predicted by Sarasola et al. [34,35], based on the binary information provided in the TCFE database (Thermo-Calc) [13,19,21] without considering ternary compounds. In addition, Mo_2B and Fe_2B were treated as a continuous series of solid solution, but it was not confirmed by any experimental investigation. Therefore, a more reliable assessment of the system should be undertaken on the basis of experimental studies along with the results obtained from the present work.

3. Experimental methods

Twenty ternary B-Fe-Mo alloys with varying B and Mo contents were prepared in a non-consumable vacuum arc-melting furnace using a non-consumable tungsten electrode under pure argon gas. The nominal composition of the alloys is given in Table 2. The raw materials are 99.99 wt% Fe grain, 99.99 wt% Mo sheet and 99.5 wt% FeB17 piece. Six grams of solidified alloys were melted at least four times to achieve homogeneity. The total mass loss of the prepared samples was kept at less than 1 wt%. Owing to the experimental difficulties caused by the high vapor pressure of B and high melting points of Mo and B, only alloys at the Fe corner were prepared and analyzed.

Microstructures of the alloys were observed using a JEOL JEM-6360LV scanning electron microscope (SEM) equipped with an energy dispersive spectrometer (EDS). The chemical compositions of the primary phases in alloys were determined by a JEOL 8630LV electron probe microanalyzer (EPMA). The constituent phases in each alloy were further identified using X-ray diffraction analysis (Rigaku Ultima IV) with Cu K_α radiation from a Ni-crystal monochromator operated at a voltage of 40 kV and current of 40 mA.

The phase transformation temperatures were determined by differential thermal analysis (DSC-NETZSCH 404 F). The heating and cooling rate is 5 K/min after the instrument calibration. DSC experiments were carried out on the samples contained within Al_2O_3 crucibles under a continuous flow of argon (99.998 wt% purity). Data for the solid-state phase transformation temperatures were determined from the heating curves, while the liquidus temperatures were taken from the cooling curves. To obtain accurate values, the analysis was carried out three times for each sample. The results of the DSC analysis are presented in Table 2.

4. Experimental results of the liquidus projection of the B-Fe-Mo ternary system

To determine the invariant reactions in the system and phase transformations during solidification, experimental investigations using SEM, EPMA, DSC and XRD were carried out for the Fe-rich alloys. Nominal compositions, thermal arrests obtained by DSC, and the suggested solidification paths of the alloys investigated are summarized in Table 2. The microstructures and solidification paths of some typical alloys were detailed below.

Alloys A1, A2, A3 and A4 locate in the primary solidification field of BCC (p_1U1E2e_2). From Fig. 3a, the primary phase in alloy A2 is dendritic BCC. Because the eutectic structure in alloy A2 is too finer to identify the phases, slow-cooling was used to obtain the distinct eutectic structure. The microstructure of alloy A2 through slow cooling from 1773 K with cooling rate of 5 K/min is shown in Fig. 3b. According to the DSC results shown in Fig. 3c, it can be conducted that the solidification started with the formation of the primary phase BCC, then followed by the monovariant formation of BCC + R reaction and finished by the eutectic reaction E2: L ⇔ BCC + τ_2 + R.

Alloy A5 locates in the primary solidification field of FCC (e_1E1U1p_1). The microstructure of the alloy A5 is shown in Fig. 4a with the matrix BCC phase, the grey block τ_1 phase, a little amount of ternary eutectic microstructure (BCC + τ_2 + Fe_2B) and finer net-like eutectoid microstructure (Fe_2B + BCC). The XRD results confirm the presence of the τ_1 phase in the sample (Fig. 4b). The eutectoid microstructure maybe form by the reaction τ_1 ⇔ Fe_2B + BCC as pointed out by Battezzati et al.[11]. Four thermal arrests were detected by DSC, which corresponds to the solidification of the primary phase FCC, the formation of eutectic reaction L⇔ FCC + τ_1 and L⇔ FCC + τ_2 + Fe_2B, and binary eutectoid reaction τ_1 ⇔ BCC + Fe_2B.

Table 2
Alloy compositions, the thermal arrests obtained by DTA and the suggested solidification paths of the Fe-Mo-B alloys.

Sample composition		Liquidus Temperature/K		Suggested reactions
		Heating	Cooling	
A1	Fe80B5Mo15	1656	1641	L→*BCC*
		-	1556	L→R + BCC
		1524	1519	L→R + BCC + τ_2
A2	Fe75B5Mo20	1640	1619	L→*BCC*
		1548	1563	L→R + BCC
		-	1516	L→R + BCC + τ_2
A3	Fe75B10Mo15	1587	1570	L→*BCC*
		-	-	L→τ_2 + BCC
		1529	1517	L + BCC→FCC + τ_2
		1341	1398	L→Fe_2B + FCC + τ_2
A4	Fe80B10Mo10	1589	1608	L→*BCC*
		-	1555	L→τ_2 + BCC
		-	-	L + BCC→FCC + τ_2
		1398	1394	L→Fe_2B + FCC + τ_2
A5	Fe80B15Mo5	1508	1491	L→*FCC*
		-	1413	L→τ_1 + FCC
		1405	1393	L→Fe_2B + FCC + τ_2
A6	Fe75B22Mo3	1442	1428	L→*Fe_2B*
		-	1411	L→Fe_2B + FCC
		1407	1400	L→Fe_2B + FCC + τ_2
A7	Fe70B28Mo3	1472	1455	L→*Fe_2B*
		-	1416	L→Fe_2B + FCC
		1398	1402	L→Fe_2B + FCC + τ_2
A8	Fe65B32Mo3	1680	1672	L→*FeB*
		1651	1643	L + FeB→Fe_2B
		-	-	L + FeB→Fe_2B + τ_2
		1387	1384	L→Fe_2B + FCC + τ_2
A9	Fe70B5Mo25	1605	1593	L→*R*
		-	-	L→R + BCC
		1535	1532	L→R + τ_2 + BCC
A10	Fe65B5Mo30	1675	1656	L→*R*
		-	1643	L→R + τ_2
		1527	1524	L→R + τ_2 + BCC
A11	Fe61B5Mo34	1720	1723	L→σ
		-	1721	L→σ + τ_2
A12	Fe65B19Mo6	1502	1485	L→τ_2
		-	1448	L→τ_2 + FCC
		1397	1394	L→Fe_2B + FCC + τ_2
A13	Fe75B15Mo10	1546	1533	L→τ_2
		-	1468	L→FCC + τ_2
		1398	1394	L→Fe_2B + FCC + τ_2
A14	Fe70B24Mo6	1630	1613	L→τ_2
		1567	1562	L→Fe_2B + τ_2
		1393	1401	L→Fe_2B + FCC + τ_2
A15	Fe70B20Mo10	1673	1658	L→τ_2
		1562	1556	L→τ_2 + FCC
		1390	1396	L→Fe_2B + FCC + τ_2
A16	Fe70B10Mo20	1593	1601	L→τ_2
		1549	1547	L→τ2 + BCC
A17	Fe65B10Mo25	1567	1552	L→τ_2
		-	-	L→R + τ_2
		1526	1523	L→R + τ_2 + BCC
A18	Fe65B15Mo20	1744	1730	L→τ_2
		-	1574	L→τ_2 + R
		1529	1526	L→R + τ_2 + BCC
A19	Fe65B25Mo10	1680	1698	L→τ_2
		1563	1560	L→τ_2 + FCC
		1397	1392	L→Fe_2B + FCC + τ_2
A20	Fe65B29Mo6	1632	1645	L→τ_2
		-		L→Fe_2B
		-	1416	L→Fe_2B + FCC
		1398	1402	L→Fe_2B + FCC + τ_2

Primary phase in italics.

Alloys A6 and A7 locate in the primary solidification field of Fe_2B (p_2U2E1e_1). The microstructure of alloy A6 is shown as Fig. 4c, which comprises dark and light grey Fe_2B, white τ_2, and matrix BCC. Solidification of alloys A6 and A7 begins with the formation of the block Fe_2B phase, continues with the formation of the binary eutectic mixture FCC and Fe_2B, and finishes with the ternary eutectic reaction E1: L ⇔ FCC + τ_2 + Fe_2B. The XRD results confirm the existence of these three phases in the sample (Fig. 4d). Therefore, the monovariant curve e_1E1 passes between alloys A5 and A6.

Alloys A9 and A10 locates in the primary solidification field of R. The microstructure of alloy A9 is shown in Fig. 5a. After the formation of R, the solidification maybe continue with the binary eutectic L ⇔ R + BCC and follows by an invariant reaction between R, τ_2 and BCC. A small thermal arrest for the binary eutectoid reaction (R ⇔ BCC + μ) was found, which takes place at about 1200 °C.

Alloys A12-A20 locates in the primary solidification field of the ternary phase τ_2. The microstructure of alloy A12 consists of the white primary τ_2 and two kinds of eutectic structures (Fig. 5b). The microstructure of alloy A12 obtained by slow cooling from 1773 K with cooling rate of 5 K/min is shown in Fig. 5c. It comprises of the block primary solidified Mo_2FeB_2 phase, white dendritic binary eutectic and finer grey eutectic microstructure (Fig. 5d). According to the microstructure and DSC results, it can be conducted that the solidification of alloy A12 begins with the formation of the Mo_2FeB_2 phase at 1502 K, then continues with formation of the monovariant eutectic L ⇔ τ_2 + FCC at 1448 K, and finishes with the formation of ternary eutectic E1: L ⇔ FCC + τ_2 + Fe_2B at 1394 K. Similar to alloy A5, the τ_1 phase was found in alloy A13. The solidification of alloy A13 begins with the formation of τ_2 phase. The second transformation corresponds to formation of the binary eutectic L ⇔ FCC + τ_2. Then solidification continues with the formation of ternary eutectic E1: L ⇔ FCC + τ_2 + Fe_2B (Fig. 5e). Alloy A18 complete the solidification with the formation of eutectic reactions L ⇔ R + τ_2 and E2: L ⇔ BCC + τ_2 + R after the formation of the primary τ_2 phase (Fig. 5f). The solidification of alloy A20 begins with the formation of τ_2, then the Fe_2B phase forms around the primary crystals (Fig. 5g). Then maybe finishes with the invariants reactions L ⇔ FCC + Fe_2B and E1:L ⇔ FCC + τ_2 + Fe_2B.

Based on the experimental results and analysis mentioned above, the liquidus projection of the B-Fe-Mo system in Fe-rich region is constructed as Fig. 6. The alloy compositions designed are indicated by different kinds of symbol according to the types of primary phase. Seven primary solidification surfaces, FCC, BCC, τ_2, Fe_2B, FeB, σ, and R, are contained in this liquidus projection, in which the τ_2 field is quiet extensive. These primary solidification surfaces are separated by the appropriate curves for joint crystallization and results in three four-phase invariant equilibria. In this region, four four-phase invariant equilibria exist including two eutectic-type, E1: L ⇔ FCC + Fe_2B + τ_2 at 1395 K; and E2: L ⇔ R + τ_2 + BCC at 1528 K, and two quasi-peritectic-type, U1: L + BCC ⇔ FCC + τ_2 at 1523 K; and U2: L + FeB ⇔ Fe_2B + τ_2 at ~ 1600 K.

5. Thermodynamic calculation of the B-Fe-Mo ternary system

5.1. Thermodynamic modeling

5.1.1. Solution phases

In the present work, the Gibbs energy functions for the unary phases of elements B, Fe, and Mo are taken from the SGTE database of pure elements [36]. B is treated as an interstitial element in iron solid solutions in this work. The solution phases FCC, BCC and HCP are described with the substitutional solution model $(Fe, Mo)_a(B, Va)_c$ and the Gibbs energy can be expressed as:

$$G^{\phi} = \sum_i y_i(y_B {}^0G^{\phi}_{i:B} + y_{Va} {}^0G^{\phi}_{i:Va}) + aRT\sum_i y_i \ln y_i + cRT(y_B \ln y_B + y_B \ln y_B) + y_{Mo}y_{Fe}(y_B L^{\phi}_{Mo,Fe:B} + y_{Va}L^{\phi}_{Mo,Fe:B}) + y_B y_{Va}\sum_i y_i L^{\phi}_{i:B,Va} + G^{\phi}_{mag} \qquad i = \text{Fe, Mo} \quad (1)$$

In Eq. (1), y stands for the site fraction of component i in the relevant sublattice. ϕ represents the FCC, BCC, and HCP phases. a and c

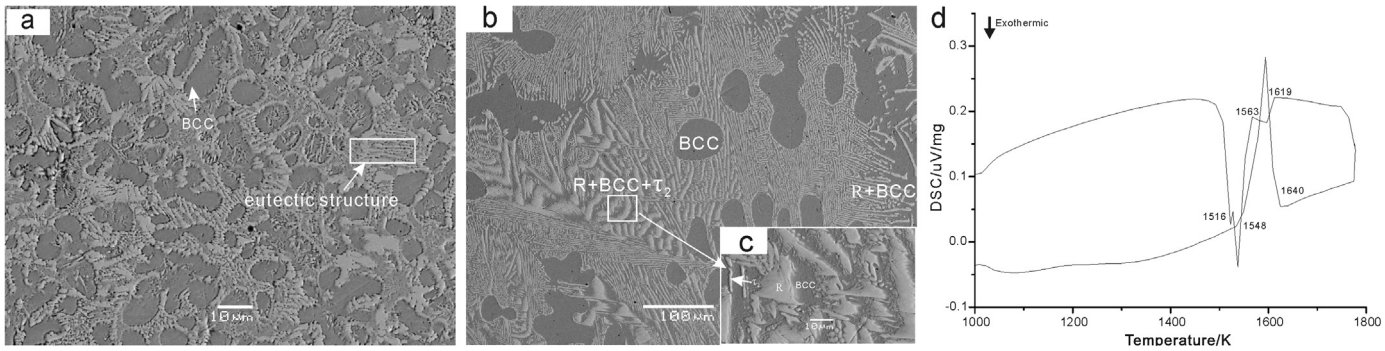

Fig. 3. As-cast microstructure of alloy A2 (a); microstructure of alloy A2 obtained by slow cooling − 5 K/min (b) and its local enlargement (c); DSC curve of alloy A2 (d).

are stoichiometric coefficients of each sublattice. R is the gas constant, and T is the temperature in Kelvin. ${}^{o}G^{\phi}_{i:\mathrm{Va}}$ is the molar Gibbs energy of pure element i in the phase, and ${}^{o}G^{\phi}_{i:\mathrm{B}}$ is the Gibbs energy of the hypothetical non-magnetic boride. $L^{\phi}_{\mathrm{Mo,Fe}:B}$ and $L^{\phi}_{\mathrm{i}:B,Va}$ are interaction parameters expressed by a Redich-Kister polynomial [37]. G^{ϕ}_{mag} is the magnetic contribution to the Gibbs energy for the BCC and FCC phases because magnetic transformation occurs in these phases. Its value is calculated according to the model of Hillert and Jarl [38].

The liquid phase is described by single sublattice where all the atoms are random mixed. Its Gibbs energy is described as follows:

$$\mathrm{G_{Liquid}} = \sum_i x_i {}^{o}G_i + RT\sum_i x_i \ln x_i + \sum_{i,j} x_i x_j L_{i,j} + \sum_{i,j,k} x_i x_j x_k L_{i,j,k} \quad (i, j, k = \mathrm{Fe,\ Mo,\ B}) \tag{2}$$

5.1.2. Stoichiometric intermetallic compounds

There are ten stable binary intermetallic compounds in the B-Fe-Mo system, Fe_2B, FeB, σ, μ, λ, R, Mo_2B, Mo_2B_5, αMoB, βMoB and Mo_2B, respectively. The solubility of the third component in each of the binary B-Fe, B-Mo, and Fe-Mo phases were found to be small. No solubility of B was found in Fe-Mo compounds, so no thermodynamic parameters for Fe-Mo compounds need to be assessed and the model parameters for Fe-Mo phases are taken from the work of Andersson et al. [26]. According to the microprobe analysis reported in the work of Leithe-Jasper et al. [30], the solubility of Mo in FeB and Fe_2B at 1323 K is about 2.5 at% and 0.6 at%, respectively. Therefore, the binary compounds Fe_2B, and FeB are treated as stoichiometric phases with two sublattices $(Fe, Mo)_a(B)_c$, and their Gibbs energy per mole are given as:

$$G_{\mathrm{Fe_aB_c}} = \sum_i y_i y_B {}^{0}G_{i:B} + aRT\sum_i y_i \ln y_i + cRT y_B \ln y_B + y_{Mo} y_{Fe} y_B L_{Mo,Fe:B} \quad (i = \mathrm{Fe,Mo}) \tag{3}$$

The solubilities of Fe in Mo_2B, βMoB and Mo_2B_5 at 1323 K are about 1.2 at%, 0.5 at% and 2.3 at%, respectively. In order to describe their solubility, the sublattice model $(Fe, Mo)_m(B, Va)_n$ is used for Mo_mB_n

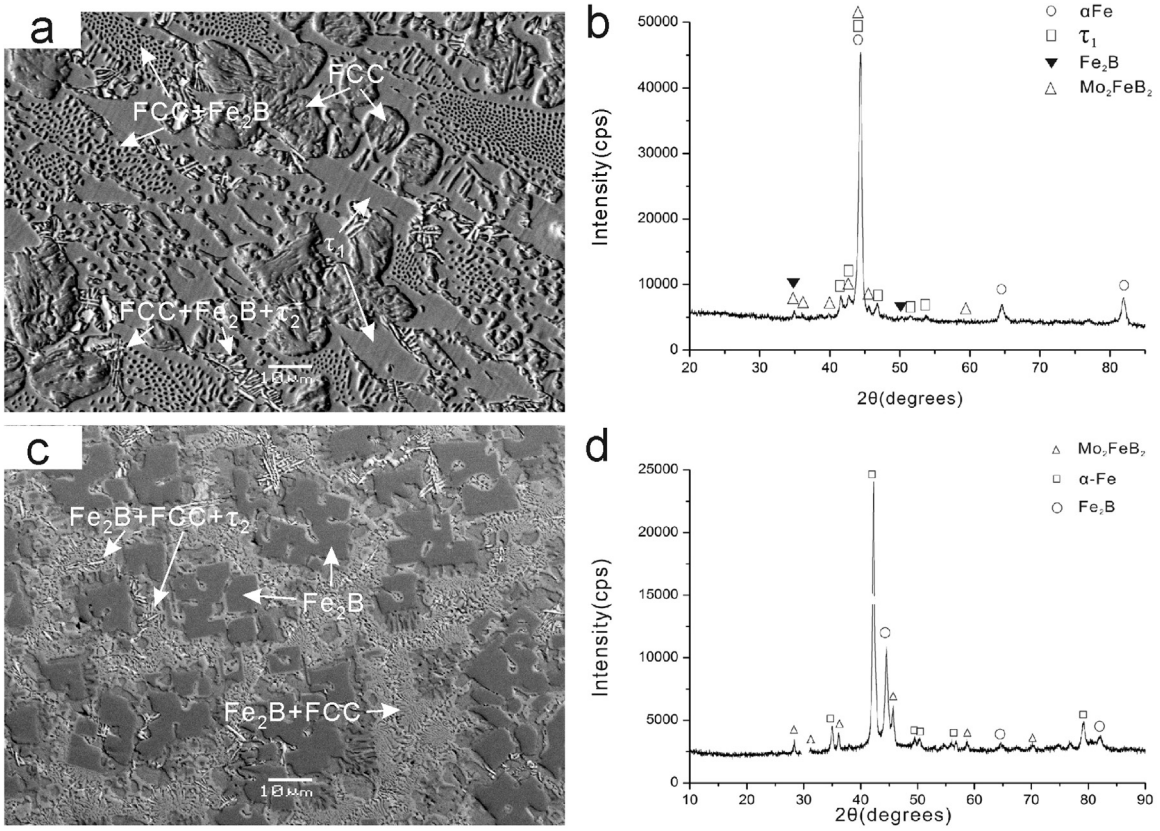

Fig. 4. The as-cast microstructures and XRD patterns of alloys A5 and A6, (a) micrograph of alloy A5; (b) XRD diffraction pattern of alloy A5; (c) micrograph of alloy A6; (d) XRD diffraction pattern of alloy A6.

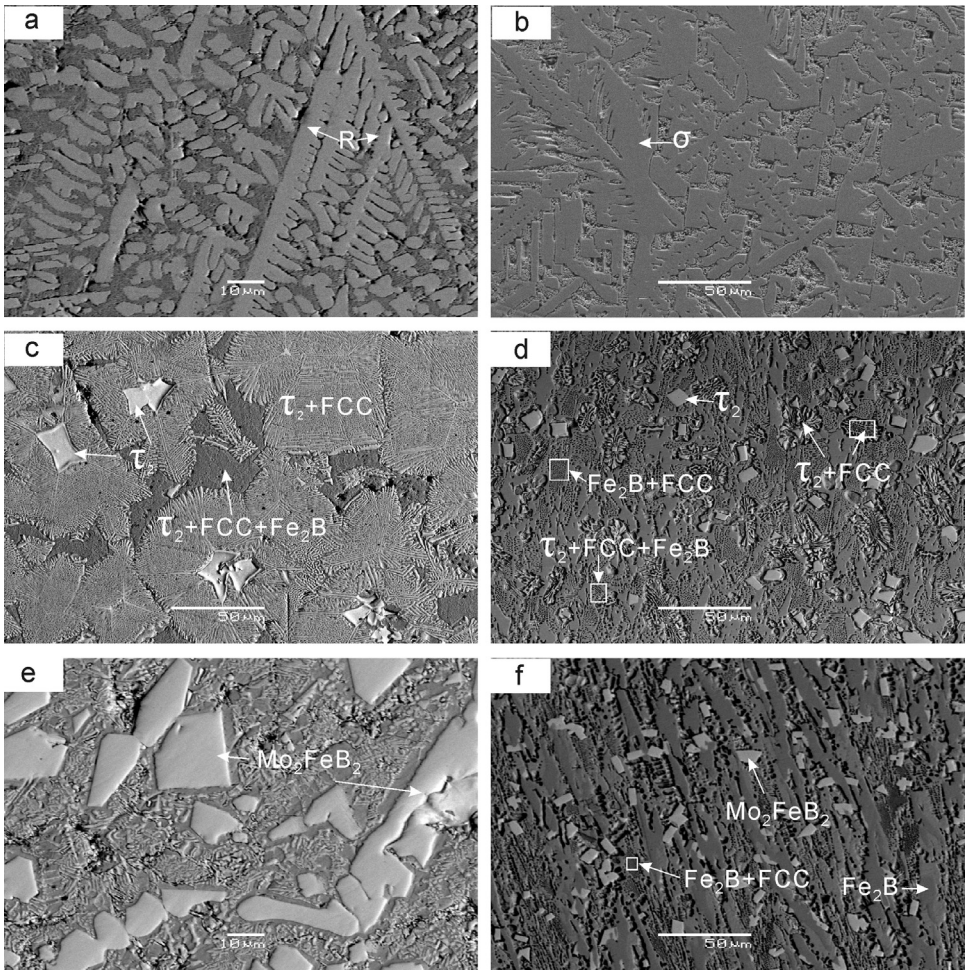

Fig. 5. Microstructures of some typical alloys (a) as-cast micrograph of A9; (b) as-cast micrograph of A12; (c) microstructure of alloy A12 obtained by slow cooling − 5 K/min (d) and its local enlargement; (e) as-cast micrograph of alloy A13; (f) as-cast microstructure of alloy A18; (g) as-cast micrograph of alloy A20.

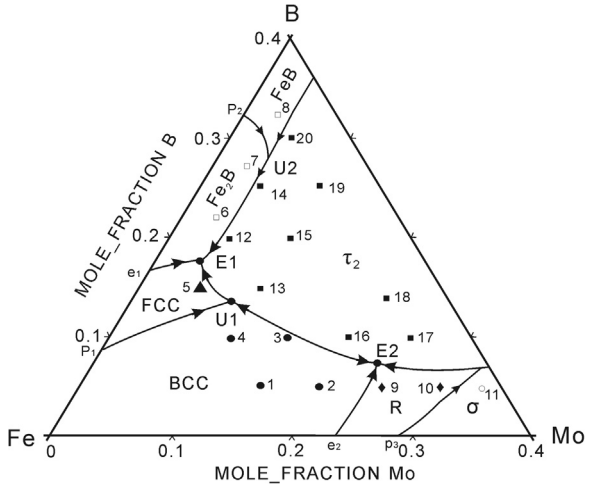

Fig. 6. Liquidus projection of the Fe-B-Mo system in the Fe-rich region.

compounds (m = 2n = 0.667 for Mo_2B, m = n = 0.5 for βMoB, and m = 0.286, n = 0.714 for Mo_2B_5). The Gibbs energies are expressed by the Eq. (1), expect for $G^{\phi}_{mag} = 0$. In addition, αMoB was considered in the recalculated phase diagram of Mo-B system, which was treated as a sublattice model $Mo_{0.5}(B, Va)_{0.5}$.

The ternary compound τ_2 with a low solubility was treated as a stoichiometric model $(B)_{0.4}(Fe)_{0.2}(Mo)_{0.4}$. Its Gibbs energy per mole of formula unit is given by:

$$G^{\phi}_{B_{0.4}Fe_{0.2}Mo_{0.4}} = 0.4^{0}G^{BetaB}_{B} + 0.2^{0}G^{Bcc,A2}_{Fe} + 0.4^{0}G^{Bcc,A2}_{Mo} + a + bT \quad (4)$$

Here, the coefficients a and b are parameters to be optimized in the present work.

5.2. Ternary compounds with composition homogeneity ranges

The composition range of τ_4 has a great change from 1323 to 1273 K. τ_4 was described as a general formula $(A, B, C)_x(A, B, C)_y(A, B, C)_z$. The model $(Fe, Mo)_{0.29}(Fe, Mo)_{0.15}(B)_{0.56}$ are used for τ_4, respectively. The Gibbs energy of them can be described by the following expression:

$$\begin{aligned} G^{\phi} = & \sum_i \sum_j \sum_k y_i^I y_j^{II} y_k^{III} {}^0G_{i:j:k} + xRT\sum_i y_i^I \ln y_i^I + yRT\sum_j y_j^{II} \ln y_j^{II} \\ & + zRT\sum_k y_k^{III} \ln y_k^{III} \\ & + \sum_{i_1,i_2} \sum_j \sum_k \left[y_{i_1}^I y_{i_2}^I y_y^{II} y_k^{III} \sum_n^k {}^nL_{i_1,i_2:j:k} \left(y_{i_1}^I - y_{i_2}^I\right)^n \right] \\ & + \sum_i \sum_{j_1,j_2} \sum_k \left[y_{i_1}^I y_{i_2}^I y_j^{II} y_k^{III} \sum_n^k {}^nL_{i:j_1,j_2}: k \left(y_{i_1}^{II} - y_{i_2}^{II}\right)^n \right] \\ & + \sum_i \sum_j \sum_{k_1,k_2} \left[y_i^I y_j^{II} y_{k_1}^{III} y_{k_2}^{III} \sum_n^k {}^nL_{i:j:k_1,k_2} \left(y_{k_1}^{III} - y_{k_2}^{III}\right)^n \right] \end{aligned} \quad (5)$$

where $G_{i:j:k}$ is the Gibbs free energy of the ϕ phase when the first sublattice is occupied by the element i (i = B, Fe, or Mo), the second by the element j (j = B, Fe, or Mo), and the third by the element k (k = B, Fe, or Mo); ${}^nL_{i_1:i_2:j:k}$ is the interaction parameter between element i_1 and

Table 3
Thermodynamic parameters in the B-Fe-Mo system.

Phase and models	Thermodynamic parameters (J mol^{-1})	Ref
Liquid: (B, Fe, Mo)$_{1.0}$	${}^{0}L_{B,Fe}^{Liquid} = -195392.47 + 82.8839075\,T(298.15–800\,K)$ $-47176.286–9.7513909\,T–59286591\,T^{-1}$ (800–6000 K)	[15]
	${}^{1}L_{B,Fe}^{Liquid} = +15272.916$, ${}^{2}L_{B,Fe}^{Liquid} = +46566.503$	[15]
	${}^{0}L_{Fe,Mo}^{Liquid} = -11712 + 2.917T$	[28]
	${}^{0}L_{B,Mo}^{Liquid} = -148828.2 + 10.9T$, ${}^{1}L_{B,Mo}^{Liquid} = -17793.3$, ${}^{2}L_{B,Mo}^{Liquid} = +21053.3$	[20]
	${}^{0}L_{B,Fe,Mo}^{Liquid} = -80861$	[O*]
BCC (Fe, Mo)$_1$(B, Va)$_3$	${}^{0}L_{Fe,Mo:\ VA}^{BCC} = +38849 - 9.539T$, ${}^{1}L_{Fe,Mo:\ VA}^{BCC} = -8988$	[28]
	${}^{0}Tc_{Fe,Mo:\ VA}^{BCC} = +334$, ${}^{1}Tc_{Fe,Mo:VA}^{BCC} = +531$	[28]
FCC: (Fe, Mo)$_1$(B, Va)$_1$	${}^{0}L_{Fe,Mo:VA}^{FCC} = +20978 - 11.843T$	[28]
FeB: (Fe, Mo)$_1$(B)$_1$	${}^{0}G_{Fe:\ B}^{FeB} = -34154.\ 2275 + 1.98158T + 0.5G_{Fe}^{BCC} + 0.5G_{B}^{BETA.RHOMBO.B}$	[28]
	$Tc_{Fe:\mathbf{B}}^{FeB} = +600$, $\beta_{Fe:\ \mathbf{B}}^{FeB} = +1.03$	[15]
	${}^{0}L_{Fe,Mo:B}^{FeB} = -193726 - 51.2T$	[O*]
Fe_2B: (Fe, Mo)$_2$B	${}^{0}G_{Fe:B}^{Fe_2B} = -27075.396 + 1.0357T + 0.667G_{Fe}^{BCC} + 0.333G_{B}^{BETA.RHOMBO.B}$	[15]
	$Tc_{Fe:\ B}^{Fe_2B} = +1018$, $\beta_{Fe:\ B}^{Fe_2B} = +1.91$	[15]
	${}^{0}L_{Fe,\ Mo:B}^{Fe_2B} = -265426 + 12.36T$	[O*]
αMoB: (Mo)$_{0.5}$(B,Va)$_{0.5}$	${}^{0}G_{Mo:\ B}^{\alpha MoB} = -54099.3177 + 1.216878T + 0.5G_{Mo}^{BCC} + 0.5G_{B}^{BETA.RHOMBO.B}$	[O*]
	${}^{0}G_{Mo:VA}^{\alpha MoB} = 5000 + 0.5G_{Mo}^{BCC}$	[O*]
	${}^{0}L_{Mo:B,VA}^{\alpha MoB} = +23866.847 + 0.5096T$	[O*]
βMoB: (Fe, Mo)$_{0.5}$(B)$_{0.5}$	${}^{0}G_{Mo:B}^{\beta MoB} = -52017 + 0.21T + 0.5G_{Mo}^{BCC} + 0.5G_{B}^{BETA.RHOMBO.B}$	[20]
	${}^{0}L_{Fe,Mo:B}^{\beta MoB} = -70676 - 27T$	[O*]
MoB_2: (Mo)$_1$(B,VA)$_2$	${}^{0}G_{Mo:B}^{MoB_2} = -123803 - 1.24658T + G_{Mo}^{BCC} + 2G_{B}^{BETA.RHOMBO.B}$	[20]
	${}^{0}G_{Mo:VA}^{MoB_2} = +13106 + G_{Mo}^{BCC}$	[20]
Mo_2B_5: (Mo, Fe)$_2$B$_5$	${}^{0}G_{Mo:B}^{Mo_2B_5} = -309004 + 21.36T + 2G_{Mo}^{BCC} + 5G_{B}^{BETA.RHOMBO.B}$	[20]
	${}^{0}G_{Mo:VA}^{Mo_2B_5} = +14545 + 2G_{Mo}^{BCC}$	[20]
	${}^{0}L_{Mo,\ Fe:B}^{Mo_2B_5} = -460900$	[O*]
MoB_4: $Mo_{0.2}B_{0.8}$	${}^{0}G_{Mo:\ B}^{MoB_4} = -32984 + 2.97T + 0.2G_{Mo}^{BCC} + 0.8G_{B}^{BETA.RHOMBO.B}$	[20]
Mo_2B : (Mo, Fe)$_{0.667}$B$_{0.333}$	${}^{0}G_{Mo:\ B}^{Mo_2B} = -42176 + 2T + 0.667G_{Mo}^{BCC} + 0.333G_{B}^{BETA.RHOMBO.B}$	[20]
	${}^{0}L_{Fe,\ Mo:\ B}^{Mo_2B} = -80000 + 5T$	[O*]
Tou 2: $Mo_{0.625}$(B,VA) $_{0.375}$	${}^{0}G_{Mo:\ B}^{Tou\ 2} = -34999 + 0.625G_{Mo}^{BCC} + 0.375G_{B}^{BETA.RHOMBO.B}$	[28]
	${}^{0}L_{Mo:\ VA}^{Tou2} = +3827 + T + 0.625G_{Mo}^{BCC}$	[28]
λ: (Fe,Mo)$_{0.667}$(Fe,Mo)$_{0.333}$	${}^{0}G_{Fe\ :\ Fe}^{\lambda} = +5000 + G_{Fe}^{BCC}$, ${}^{0}G_{Mo:Mo}^{\lambda} = +5000 + G_{Mo}^{BCC}$	[28]
	${}^{0}G_{Fe\ :\ Mo}^{\lambda} = -6814.33 + 2.43T + 0.667G_{Fe}^{BCC} + 0.333G_{Mo}^{BCC}$	[28]
	${}^{0}G_{Mo\ :\ Fe}^{\lambda} = +16814.33 - 2.43T + 0.333G_{Fe}^{BCC} + 0.667G_{Mo}^{BCC}$	[28]
	${}^{0}L_{Fe:\ Fe,\ Mo}^{\lambda} = +23333.\ \ 33$, ${}^{0}L_{Fe,\ Mo:\ \ Mo}^{\lambda} = +19816.67$	[28]
μ: (Fe,Mo)$_{0.461}$(Fe,Mo)$_{0.154}$Mo$_{0.308}$(Fe,Mo) $_{0.077}$	${}^{0}G_{Fe:\ \ Fe\ :Mo:\ \ Fe}^{\mu} = +5699.23 - 5.898T + 0.692G_{Fe}^{BCC} + 0.308G_{Mo}^{BCC}$	[28]
	${}^{0}G_{Mo:\ \ Fe\ :Mo:\ \ Fe}^{\mu} = +34303.846 + 0.23G_{Fe}^{BCC} + 0.77G_{Mo}^{BCC}$	[28]
	${}^{0}G_{Fe:\ \ Mo\ :Mo:\ \ Fe}^{\mu} = -5298.077 + 0.689T + 0.538G_{Fe}^{BCC} + 0.462G_{Mo}^{BCC}$	[28]
	${}^{0}G_{Mo:\ \ Mo:Mo:\ \ Fe}^{\mu} = +26227.69 + 0.077G_{Fe}^{BCC} + 0.923G_{Mo}^{BCC}$	[28]
	${}^{0}G_{Fe::\ Fe:\ Mo:\ Mo}^{\mu} = +7760.77 + 0.615G_{Fe}^{BCC} + 0.385G_{Mo}^{BCC}$	[28]
	${}^{0}G_{Mo:\ \ Fe:\ Mo:\ Mo}^{\mu} = +37290 + 0.154G_{Fe}^{BCC} + 0.846G_{Mo}^{BCC}$	[28]
	${}^{0}G_{Fe\ :Mo:\ Mo:\ Mo}^{\mu} = +1811.538 + 0.462G_{Fe}^{BCC} + 0.538G_{Mo}^{BCC}$	[28]
	${}^{0}G_{Mo:\ \ Mo:\ Mo:\ Mo}^{\mu} = +30380 + G_{Mo}^{BCC}$, ${}^{0}L_{Fe:\ \ Fe,\ Mo:\ Mo:\ Fe}^{\mu} = -10577.69 + 8.084T$	[28]
R: (Fe, Mo)$_{0.60}$Mo$_{0.34}$(Fe, Mo)$_{0.06}$	${}^{0}G_{Fe:\ Mo:\ \ Fe}^{R} = +960.547 - 3.345T + 0.66G_{Fe}^{BCC} + 0.34G_{Mo}^{BCC}$	[28]
	${}^{0}G_{Fe:\ Mo:\ \ Mo}^{R} = -1726.377 - 1.512T + 0.60G_{Fe}^{BCC} + 0.4G_{Mo}^{BCC}$	[28]
σ: (Fe, Mo)$_{0.333}$(Fe, Mo)$_{0.667}$	${}^{0}G_{Fe:\ Fe}^{\sigma} = +7550 + G_{Fe}^{BCC}$, ${}^{0}L_{Mo:\ Mo}^{\sigma} = +16230 + G_{Mo}^{BCC}$	[28]
	${}^{0}G_{Fe:\ Mo}^{\sigma} = +1046.9 - 1.4627T + 0.333G_{Fe}^{BCC} + 0.667G_{Mo}^{BCC}$	[28]
	${}^{0}G_{Mo:\ Fe}^{\sigma} = +16263.33 + 0.667G_{Fe}^{BCC} + 0.333G_{Mo}^{BCC}$, ${}^{0}L_{Fe:\ Fe,\ Mo}^{\sigma} = -1603.8$	[28]

(*continued on next page*)

Table 3 (*continued*)

Phase and models	Thermodynamic parameters (J mol^{-1})	Ref
τ_1: $Fe_{0.7}Mo_{0.05}B_{0.25}$	${}^{0}G^{\tau 1}_{Fe:Mo:B} = -23383 + 1.17T + 0.7G^{BCC}_{Fe} + 0.05G^{BCC}_{Mo} + 0.25G^{BETA.RHOMBO.B}_{B}$	[O*]
τ_2: $Fe_{0.2}Mo_{0.4}B_{0.4}$	${}^{0}G^{\tau 2}_{Fe:Mo:B} = -49500 + 0.2G^{BCC}_{Fe} + 0.4G^{BCC}_{Mo} + 0.4G^{BETA.RHOMBO.B}_{B}$	[O*]
τ_4: $(Fe, Mo)_{0.29}Mo_{0.15}B_{0.56}$	${}^{0}L^{\tau 4}_{Fe:Mo:B} = -50900 + 6.8T + 0.29G^{BCC}_{Fe} + 0.15G^{BCC}_{Mo} + 0.56G^{BETA.RHOMBO.B}_{B}$	[O*]
	${}^{0}G^{\tau 4}_{Mo:Fe:B} = -37000 - 7T + 0.18G^{BCC}_{Fe} + 0.26G^{BCC}_{Mo} + 0.56G^{BETA.RHOMBO.B}_{B}$	[O*]
	${}^{0}L^{\tau 4}_{Fe,Mo:Mo:B} = -87500$	[O*]

O*- parameter optimized in this work.

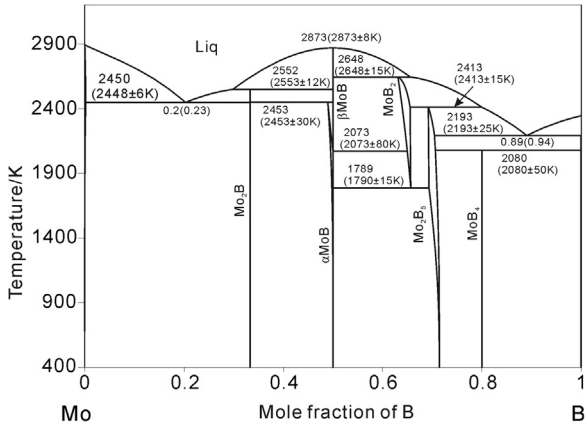

Fig. 7. Calculated phase diagrams of the Mo-B system. The experimental data in parenthesis come from Spear and Liao [18].

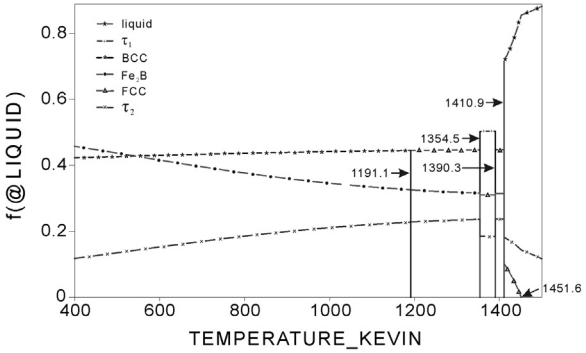

Fig. 9. Calculated solidification path of the alloy (Fe70B20Mo10).

i_2 (i_1, i_2 = B, Fe or Mo and $i_1 \neq i_2$) when the second sublattice is occupied by the element j (j = B, Fe or Mo), and the third by the element k (k = B, Fe or Mo); The parameters ${}^{n}L_{i:j_1:j_2:k}$ and ${}^{n}L_{i:j:k_1:k_2}$ are described in the same way.

5.3. Calculation results and discussion

Based on the experimental results of Leithe-Jasper et al.[30], βMoB is stabilized by dissolving Fe. In addition, αMoB and βMoB were found to co-exist at 1323 K. However, the reported modeling for Mo-B system can't describe two modifications of MoB. Therefore, Mo-B phase diagram was reassessed based on the parameters reported by Yang et al. [20]. The model parameters are listed in Table 3. The calculated Mo-B phase diagrams is shown in Fig. 7. The values in parentheses are the experimental values obtained from [18]. Two invariant reactions βMoB + Mo_2B ↔ αMoB at 2453 ± 50 K, and L + βMoB ↔ Mo_2B, at 2553 ± 12 K were well described.

The thermodynamic parameters of the phases in the B-Fe-Mo system were assessed using the Thermo-Calc software, based on phase equilibria along with thermodynamic data. The experimental data of phase equilibria at 1273 K and 1323 K as well as the liquidus projection of the Fe-rich corner were used to assess the B-Fe-Mo system. A summary of the thermodynamic parameters in this work are listed in Table 3. A comparison between the calculated and the experimental phase relations at 1273 K and 1323 K is presented in Fig. 8. The results show that

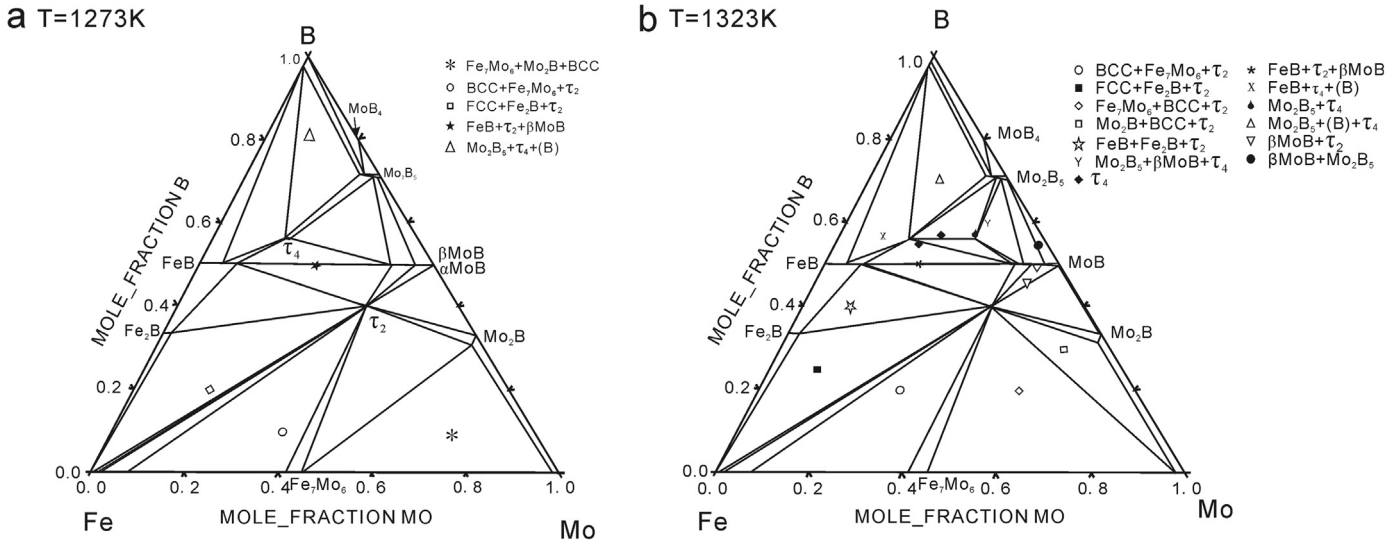

Fig. 8. Calculated isothermal sections of the B-Fe-Mo system at 1273 K superimposed with the experimental data from Gladyshevskii et al. [32] (a); and that at 1323 K superimposed with the experimental data from Leithe-Jasper et al. [30] (b).

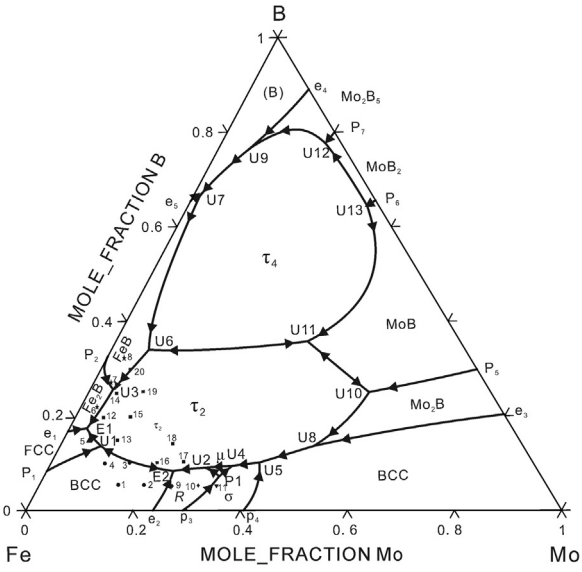

Fig. 10. Calculated liquidus surface projection of the B-Fe-Mo system over the whole composition range marked with experimental data obtained in the present work.

Table 4
Calculated invariant reactions with the available data in the B-Fe-Mo system.

Invariant reactions	Type	Temperature/K	Liquid composition (at%)		
			Fe	Mo	B
L + βMoB ⇔τ_4 + MoB_2	U13	2619.1	2.5	33.2	64.3
L + MoB_2 ⇔ τ_4 + Mo_2B_5	U12	2398.0	2.5	19.6	77.9
L + βMoB ⇔τ_2 + τ_4	U11	2337.7	32.6	32.3	35.1
L + βMoB ⇔ τ_2 + Mo_2B	U10	2215.6	24.7	50.3	25.0
L + Mo_2B_5 ⇔ τ_4 + (B)	U9	2135.4	11.2	8.6	80.2
L + Mo_2B ⇔ τ_2 + BCC	U8	1829.6	40.0	46.2	13.8
L + τ_4 ⇔ (B) + FeB	U7	1794.8	35.3	0.9	63.8
L + τ_4 ⇔ τ_2 + FeB	U6	1735.7	60.7	6.1	34.2
L + BCC ⇔τ_2 + σ	U5	1645.5	51.2	38.5	10.3
L + R + σ ⇔ μ	P1	1644.5	60.0	32.7	7.2
L + σ ⇔ μ + τ_2	U4	1603.1	56.1	34.2	9.7
L + FeB ⇔ τ_2 + Fe_2B	U3	1593.4	67.5	4.6	27.9
L + μ ⇔ R + τ_2	U2	1570.2	61.9	28.8	9.3
L + BCC ⇔ τ_2 + FCC	U1	1514.5 1523[a]	77.6	8.1	14.3
L ⇔ R + τ_2 + BCC	E2	1530.5 1528[a]	67.5	23.9	8.6
L ⇔ τ_2 + FCC + Fe_2B	E1	1410.9 1395[a] 1365–1405 [33]	78.5	3.7	17.8

[a] Experimental value obtained in this work, otherwise the calculation.

the thermodynamic modeling can reproduce the experimental results very well. In the calculated isothermal section, the solubility of the third elements in the binary compounds was considered. The solidification path of the alloy (Fe70B20Mo10) was calculated, and the result is shown in Fig. 9. The L ⇔ τ_2 + L ⇔ L + FCC + τ_2 ⇔ FCC + τ_2 + Fe_2B ⇔ FCC + τ_1 + τ_2 ⇔ FCC + τ_2 + Fe_2B ⇔ BCC + τ_2 + Fe_2B solidification process would take place. The calculated result indicates that the τ_1 phase is stable only at a narrow temperature range from 1354.3 to 1390.3 K, lower than the lowest temperature of the existence range of liquid. So τ_1 phase don't have a field of primary crystallization in the liquidus surface.

Fig. 10 presents the calculated liquidus projection of the B-Fe-Mo system over the whole composition range. The calculated invariant ternary reactions involving liquid are tabulated in Table 4, along with the experimental results obtained in this work listed for comparison. The calculated results showed that two eutectic, one peritectic and thirteen quasi-peritectic four-phase invariant equilibrium reactions may

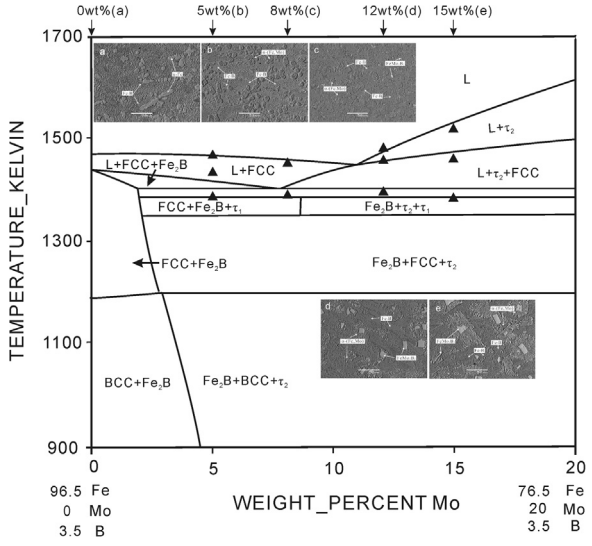

Fig. 11. Calculated vertical section with B fixed at 3.5 wt% compared with the DSC results.

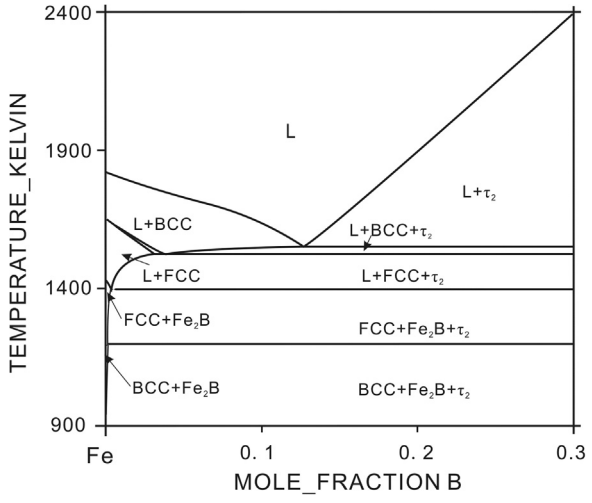

Fig. 12. Calculated vertical section along the Fe-τ_2 join.

take place.

As mentioned at beginning, the addition of Mo in Fe-3.5B alloy can improve the corrosion resistance of alloy in the molten zinc. In order to provider a guidance for understanding the effect of the Mo on the microstructure of the Fe-B alloy and verifying the applicability of thermodynamic parameters obtained in this work, a partial vertical section with B fixed at 3.5 wt% was determined experimentally by using SEM and DSC. Five as-cast Fe-3.5B alloys with various Mo contents (0, 5, 8, 12, and 15 wt%) were prepared and analyzed. In the Fe-3.5B-5Mo and Fe-3.5B-8 alloys, the L → L + FCC → L + FCC + Fe_2B → τ_2 + Fe_2B + FCC → τ_1 + Fe_2B + FCC → τ_2 + Fe_2B + FCC → τ_2 + Fe_2B + BCC solidification process takes place. The solidification process for the alloy containing 12 and 15 wt% Mo is L → L + τ_2 → L + τ_2 + FCC → τ_2 + Fe_2B + FCC → τ_1 + Fe_2B + FCC → τ_2 + Fe_2B + FCC → Fe_2B + τ_2 + BCC. Therefore, with the increasing Mo addition, the primary phases change from FCC to τ_2. Based on the thermodynamic parameter obtained by the present work, the vertical section with B fixed at 3.5 wt % is calculated as Fig. 11, in which the experimental data obtained in this work are marked with triangles. The calculated ternary eutectic composition in this vertical section is 7.47 wt% Mo. The alloy with the composition closed to the eutectic point shows the best corrosion resistance to molten zinc according to previous work [9].

τ_2-Mo_2FeB_2 is a very important ternary boride, which can be used as

wear-resistance materials. The vertical section of Fe-τ_2 can provide guidance for the sintering of Mo_2FeB_2-based cermets. Fig. 12 shows the calculated vertical section along the Fe-τ_2 join (Mo:B = 1). As can be seen, the primary τ_2 phase would form when the Mo content is more than 12.5 at%, and liquid begins to form above 1395 K. In summary, since the experimental data of the B-Fe-Mo system is limited, further investigation are needed for clarification. The results of the present study might provide guidance for future studies.

6. Conclusion

The liquidus projection of the B-Fe-Mo system in the Fe-rich region has been determined experimentally. Two ternary eutectic reactions were identified in the region of study: E1: L ⇔ FCC + Fe_2B + τ_2 at 1395 K; and E2: L ⇔ R + τ_2 +BCC at 1528 K. The system is characterized by the dominance of the ternary compound τ_2. Based on the available literature for thermodynamic assessments of the Fe-B, Fe-Mo, and B-Mo binary systems and experimental data, a set of thermodynamic parameters have been obtained in present work. The calculated results and most of the experimental data are in good agreement.

Acknowledgments

This work was supported by the National Science Foundation of the China (No. 51471141, 2015), the Key Project of the Education Department of Hunan Province (No. 15A179), and the Scientific Research Fund of Hunan Provincial Educational Department (No. 2016JC2005, 2016).

References

[1] C. Liu, M. Madinehei, E. Pineda, D. Crespo, J. Therm. Anal. Calorim. 125 (2) (2016) 711–719.
[2] Y. Li, X. Cui, Z. Luo, S. Ao, J. Mater. Eng. Perform. (2016) 1–7.
[3] J.Y. Cheng, A.M. Zhao, Y.L. Chen, et al., Mater. Sci. Technol. 20 (4) (2012) 38–44.
[4] C. Suryanarayana, A. Inoue, Int. Mater. Rev. 58 (2013) 131–166.
[5] M. Madinehei, P. Bruna, M.J. Duarte, E. Pineda, J. Klemm, F.U. Renner, J. Alloy. Compd. 615 (2014) 128–131.
[6] V. Ponnambalam, S. Joseph Poonand Gary, J. Shiflet, S.J. Poon, A.G.J. Shiflet, J. Mater. Res. 19 (10) (2004) 3046–3052.
[7] F. Yang, Y. Wu, J. Han, et al., J. Alloy. Compd. 665 (2016) 373–380.
[8] X. Ren, L. Yu, Y. Liu, et al., Int. J. Refract. Met. Hard Mater. 61 (2016) 207–214.
[9] X. Ouyang, F. Yin, G. Chen, M. Zhao, Y. Liu, Corrosion 73 (8) (2017) 942.
[10] Y. Khan, E. Kneller, M. Sostarich, Z. Metallkd. 73 (1982) 624.
[11] L. Battezzati, C. Antonione, J. Alloy. Compd. 247 (1997) 164–171.
[12] T.V. Rompaey, K.C.H. Kumar, P. Wollants, J. Alloy. Compd. 334 (1) (2002) 173–181.
[13] B. Hallemans, P. Wollants, J.R. Roos, Z. Metallkd. 85 (1994) 676.
[14] K. Yoshitomi, Y. Nakama, H. Ohtani, M. Haeebe, ISIJ Int. 48 (2008) 835.
[15] M. Palumbo, G. Cacciamani, E. Bosco, et al., Calphad 25 (4) (2001) 625–637.
[16] L. Brewer, R.H. Lamoreaux, At. Energy Rev. Spec. 18 (7) (1980).
[17] K.E. Spear, M.S. Wang, Calphad 5 (2) (1981) 109–113.
[18] K.E. Spear, P.K. Liao, Bull. Alloy Phase Diagr. 9 (1988).
[19] M. Morishita, K. Koyama, S. Yagi, G. Zhang, J. Alloy. Compd. 314 (2001) 212–218.
[20] Y. Yang, Y.A. Chang, Intermetallics 13 (2) (2005) 121–128.
[21] A.F. Guillermet, Bull. Alloy Phase Diag. 33 (1982) 359–367.
[22] T.B. Massalski, H. Okamoto, P.R. Subramanian, L. Kacprzak, Binary Alloy Phase Diagrams, 2nd edition, ASM International. Metarials park, Ohio, USA, 1990.
[23] L. Kaufman, H. Nesor, Calphad 2 (55) (1978) 55–80.
[24] H.D. Nussler, T. Hoster, O. Kubaschewski, Z. Metallkd. 71 (1980) 396–397.
[25] A.F. Guillermet, Calphad 6 (2) (1982) 127–140.
[26] J.O. Andersson, N. Lange, Metall. Mater. Trans. A 6 (1988) 1385–1394.
[27] J. Houserová, J. Vřešťál, M. Šob, Calphad 29 (2) (2005) 133–139.
[28] V.B. Rajkumar, K.C.H. Kumar, J. Alloy. Compd. 611 (2014) 303–312.
[29] H. Haschke, H. Nowotny, F. Benesovsky, Mon. Chem. 97 (1966) 1459–1468.
[30] A. Leithe-Jasper, H. Klesnar, P. Rogl, M. Komai, K.I. Takagi, J. Jpn. Inst. Met. 64 (2) (2000) 154–162.
[31] K. Korniyenko, A. Bondar, Refractory Metal Systems, Springer, 2009, pp. 680–694.
[32] E.I. Gladyshevskii, T.F. Fedorov, B.Y. Kuz'ma, R.V. Skolozdra, Poroshk. Metall. 4 (1966) 55–60.
[33] T. Ide, T. Ando, Metall. Trans. A 20 (1) (1989) 17–24.
[34] M. Sarasola, T. Gómez-Acebo, F. Castro, Acta Mater. 52 (2004) 4615–4622.
[35] M. Sarasola, T. Gómez-Acebo, F. Castro, Powder Met. 48 (1) (2005) 59–67.
[36] SGTE pure elements (unary) database, version 5.1 Scientific Group Thermodata Europe, Teddington, UK, 2010.
[37] O. Redlich, A. Kister, Ind. Eng. Chem. 40 (1948) 345.
[38] M. Hillert, M. Jarl, Calphad 2 (1978) 227–238.